Dawson-type polyoxometalates photosensitized with carbon dots for **photocatalytic reduction of silver ions**

Antonino Madonia[1], Mercè Martin-Sabi[1], Aymène Sadaoui[1], Laurent Ruhlmann[2], Souad Ammar[1] and Delphine Schaming[1,]*

[1] Université de Paris, ITODYS, UMR 7086 CNRS, 15 rue Jean-Antoine de Baïf, 75013 Paris, France

[2] Université de Strasbourg, Institut de Chimie, UMR 7177 CNRS, 4 rue Blaise Pascal, 67000 Strasbourg, France

Abstract

Carbon dots (CDs) are carbon-based nanoparticles (NPs) displaying remarkable light-harvesting properties. In this work, we have investigated for the first time the possibility to use CDs to photosensitize polyoxometalates (POMs). For this purpose, we have thus engineered positively charged carbon dots allowing electrostatic interactions with anionic Dawson-type POMs. Following the formation of these new POM-CDs complexes, an efficient photoinduced electron transfer between photoexcited CDs and POMs allows the reduced POM to perform reduction reactions. The reduction of silver ions into silver nanoparticles (AgNPs) has been chosen as a model reaction.

Keywords

Carbon dots – Polyoxometalates – Photosensitizers – Photocatalysis – Silver nanoparticles

1. Introduction

Photocatalytic processes currently attract an extremely wide scientific interest [1–3]. This is motivated by the powerful potential applications in tackling many important environmental and energy challenges at a global level. Indeed, many new photocatalysts which are developed and engineered are tailored in an economically sustainable manner and are able to perform different processes such as the degradation of pollutants [4,5] and the generation of green energy [6,7]. In particular considerable efforts are devoted to the enhancement of the photocatalytic activity of several materials, with the target of optimizing the use of solar energy. While the most effective photocatalysts are generally active only in the UV-domain, a useful approach consists in combining photocatalysts with photosensitizers so to harvest visible light. Commonly used photosensitizers include molecular dyes, metal and semiconductor nanoparticles [8,9]. Nevertheless, organic dyes generally possess limited photostability while inorganic sensitizers often contain precious metals. In addition, while semiconductor nanoparticles such as quantum dots are often more photostable than molecular dyes, they are generally regarded as toxic. Thus, a key requirement for achieving a sustainable photocatalytic system is the development of efficient environmentally-friendly and low-cost light harvesters.

Carbon dots (CDs) constitute an emerging class of optically active carbon nanomaterials discovered only a few years ago [10,11]. They are small (generally less than 10 nm) carbon based and highly surface-functionalized nanoparticles, displaying very bright fluorescence and intense absorption bands often covering most of the visible domain. Moreover, they are not expensive to synthesize and have low toxicity, but most importantly they possess excellent photostability. As a consequence, CDs are often regarded as a promising alternative to molecular dyes and semiconductor particles for a wide range of applications especially as photosensitizers in photocatalytic processes.

Despite their promising properties, CDs are currently under-explored in photocatalytic applications. Several studies have focused on the coupling of CDs with semiconductors (TiO_2, CoO, Cu_2O, Fe_2O_3…) where the role of CDs to enhance their photocatalytic activity is undeniable [12–17]. Indeed, CDs can

promote interfacial charge carrier separation of semiconductors and consequently decrease charge-carrier recombinations [18]. Moreover, similarly to other carbon materials, they can also increase the conductivity of semiconductors [19,20]. However, a photosensitizing effect with a clear proof of an electron transfer between the excited CDs and the photocatalyst has yet to be shown.

In this context, we have very recently reported the evidence of a spontaneous electrostatic coupling between positively charged CDs and a Dawson-type POM, the $[P_2W_{18}O_{62}]^{6-}$ anion [21]. Ultrafast transient absorption spectroscopy has allowed to evidence within this CDs-POM hybrid a highly efficient electron transfer resulting in a charge-separated state formed within 120 fs from photo absorption. Additionally, POMs are known as UV photocatalysts able to exchange rapidly and reversibly a large number of electrons [22–29], and as visible light photocatalysts when coupled to judicious photosensitizers to enhance their solar harvesting efficiency [30–35]. As a consequence, we believe these new CDs-POM nanohybrids to be very promising for photocatalytic applications, in particular for reduction processes.

As a proof of concept, we have investigated the photoreduction of silver ions using CDs coupled with several Dawson-type POMs. Indeed, the photoreduction of silver ions is often chosen as a model reaction for photocatalyst tests, particularly when using POMs: in fact such a reaction is already well documented and the underlying mechanism well described under UV illumination [22].

2. Experimental section

2.1. Synthesis of CDs

The synthesis procedure of CDs was adapted from the literature [36]. 250 mg of crushed down crystalline pyrene powder were dispersed in 20 mL of 70% HNO_3. The mixture was then heated overnight at 80°C under reflux and vigorous stirring in order to proceed to the nitration of the pyrene. The resulting 1,3,6-trinitropyrene was recovered as a yellow powder *via* vacuum filtration and then mixed to a 75 mL of 0.4 M ammonia and 1.5 M hydrazine aqueous solution. The mixture was sonicated for 1 hour before

its transfer into a 125 mL Teflon-lined autoclave. The sealed autoclave is then placed into a 200°C oven overnight. The obtained CDs were finally separated from unreacted carbonaceous material through vacuum filtration **and were obtained with a yield of 75%**.

2.2. Synthesis of POMs

$K_6[P_2W_{18}O_{62}]$ and $Na_{12}[\alpha\text{-}P_2W_{15}O_{56}]$ (used for the synthesis of Dawson-derived sandwich POMs) were prepared according the method published by Contant [37]. **$K_6[P_2W_{18}O_{62}]$ was obtained with a yield of 70%.**

Tetranuclear Dawson-derived sandwich POMs were synthesized according a protocol adapted from Finke *et al.*[38].

$Na_{16}[Co_4(H_2O)_2(P_2W_{15}O_{56})_2]\cdot 51H_2O$: $Co(NO_3)_2.6H_2O$ (0.73 g, 2.25 mmol) was dissolved in 50 mL of 1 mol L^{-1} aqueous solution of NaCl. $Na_{12}[\alpha\text{-}P_2W_{15}O_{56}]\cdot 24H_2O$ (5.00 g, 1.13 mmol) was then added and dissolved by heating and stirring. The original light pink solution became a homogeneous red-brown solution that reflected green. The solution was then cooled at 5 °C overnight. Patches of a crystalline green-brown product formed on cooling. When collected, the product lost its crystalline form and immediately became an amorphous green-brown solid. The product was dried at 60 °C under vacuum for 30 min. Yield: 83% (3.99 g, 0.46 mmol). ^{31}P NMR (D_2O): δ = 6.8 and 1483 ppm.

$Na_{16}[Zn_4(H_2O)_2(P_2W_{15}O_{56})_2]\cdot 50H_2O$: $ZnCl_2$ (0.32 g, 2.35 mmol) was dissolved in 1 mol L^{-1} of aqueous solution of NaCl (50 mL) with stirring. $Na_{12}[\alpha\text{-}P_2W_{15}O_{56}]\cdot 24H_2O$ (5.00 g, 1.13 mmol) was then slowly added under vigorous stirring. The solution was heated at 60°C for 15 min and then filtered hot. The white crystalline solid collected was then dried in air. Yield: 87% (4.59 g, 0.51 mmol). ^{31}P NMR (D_2O): δ = -13.95 and -3.92 ppm.

2.3. Photocatalysis experiments

Irradiation was performed using a 500 W-Xe lamp equipped with an optical fiber, an IR and an UV cut-off filters to avoid warming of the solution and direct photoactivation of POMs. The samples consisted of 4 mL of aqueous solutions of Ag_2SO_4 (4×10^{-5} mol L^{-1}), POM (10^{-5} mol L^{-1}), CDs (25 **mg L^{-1}**) and propan-2-ol (0.13 mol L^{-1}) in a quartz cuvette of 1 cm path length. The pH was adjusted to 4 using HCl to ensure the electrostatic interaction between POMs and positively charged CDs. Solutions were finally deaerated by bubbling argon and then sealed. All experiments were carried out at room temperature.

UV-vis absorption spectra were obtained on a Perkin Elmer LAMBDA 1050 spectrophotometer. Transmission electronic microscopy (TEM) observations were performed with a JEOL 100 CXII TEM instrument operated at an accelerating voltage of 100 kV.

3. Results and discussion

3.1. Characterization of CDs

CDs were synthetized by hydrothermal method using trinitropyrene in a reducing medium in order to obtain CDs with amine groups attached to their surface. High-resolution transmission electronic microscopy (HR-TEM) images of the obtained CDs are shown in Fig. 1, displaying dots approximately sized 5 nm. The contrast of the images is poor due to the use of TEM copper grids coated with amorphous carbon. Nonetheless, we can distinguish lattice planes and the Fast Fourier Transform (FFT) of the images was calculated to investigate the CDs core structure. The measurements revealed lattice spacings of 2.1, 2.5 and 2.9 Å, which are consistent with diffraction planes generally observed for CDs [39].

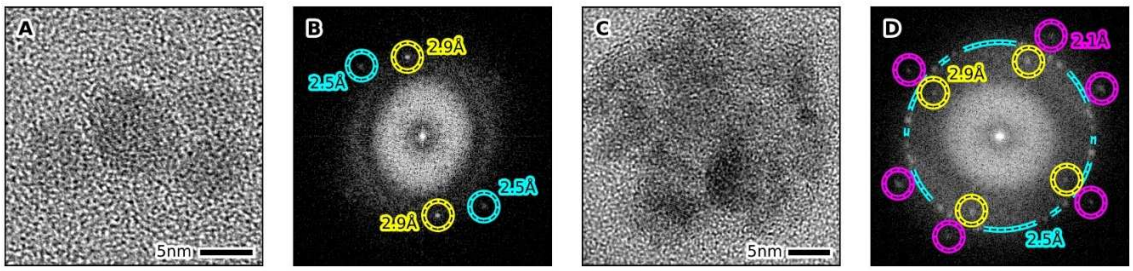

Fig. 1. A and C) HRTEM images of CDs; **B and D)** FFT respectively calculated from (A) and (C); the planar distances responsible for the observed diffraction peaks are indicated.

In acidic medium, the amine groups attached to the surface of the CDs can be easily protonated leading to positively charged ammonium groups. The electrophoretic mobility of CDs was measured before and after acidification to observe the changes in surface charge due to the change of the protonation state of the organic groups present on the CDs surface. The resulting ζ-potential distributions measured at pH 9.8 and 4 are shown in Fig. 2. It appears that the ζ-potential value can be tuned from -18.5 mV to +10.3 mV by decreasing the pH of the solution. As a consequence, in acidic conditions, we obtain positively charged CDs which can ensure electrostatic interactions with anionic POMs.

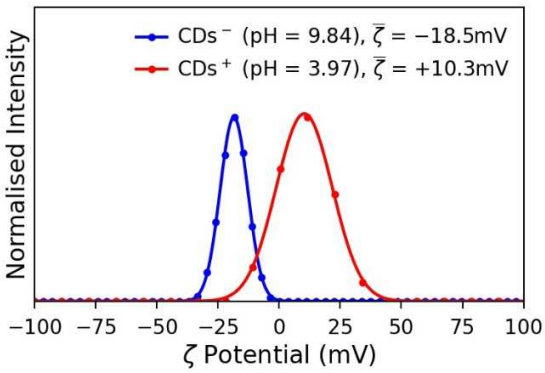

Fig. 2. ζ-potential distributions displayed by CDs at pH 9.8 and 4.

3.2. Fluorescence evidence of the interaction between POM and CDs

Following the previous results, in all experiments the pH of CDs solutions was adjusted to 4, so to ensure the protonation of organic moieties present on the nanoparticles surface. As observed in Fig. 3. A, the fluorescence intensity of positively charged CDs rapidly decreases upon addition of $[P_2W_{18}O_{62}]^{6-}$ (indicated as $\{P_2W_{18}\}$). This quenching has been recently described as the result of a fast electron transfer between the excited CDs and the POM, which has been studied in details elsewhere [21]. Similar behavior has been observed for the two other POMs used in this study, namely $[Co_4(P_2W_{15}O_{56})_2]^{16-}$ ($\{Co_4P_4W_{30}\}$) and $[Zn_4(P_2W_{15}O_{56})_2]^{16-}$ ($\{Zn_4P_4W_{30}\}$), as evidenced by the strong quenching of the fluorescence of the CDs upon addition of these two tetranuclear Dawson-derived sandwich POMs (Fig. 3. B and C).

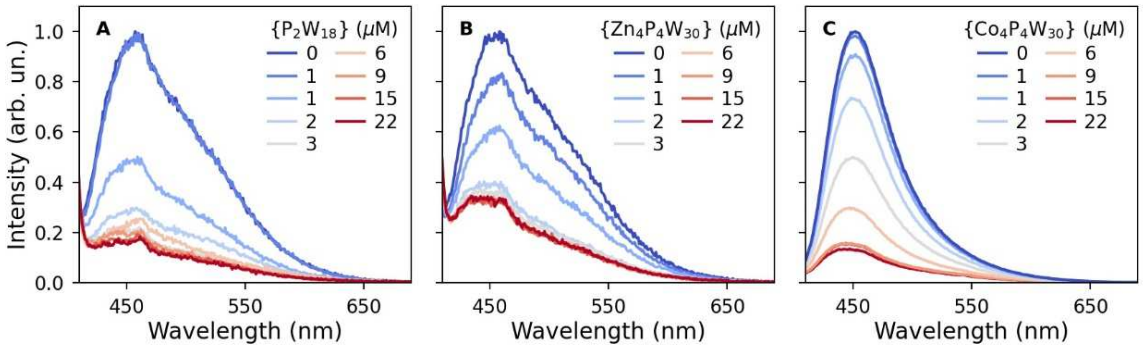

Fig. 3. Emission spectra of CDs at pH 4 after addition of **A)** $\{P_2W_{18}\}$, **B)** $\{Zn_4P_4W_{30}\}$ and **C)** $\{Co_4P_4W_{30}\}$ at the indicated concentrations.

3.3. Photoreduction of Ag^+ ions using CDs/$\{P_2W_{18}\}$ complex

Experiments were performed on aqueous CDs/$\{P_2W_{18}\}$ solutions obtained at a POM concentration equal to 10 µM. 8 equivalents of Ag^+ ions compared to POM were added to the solution previously acidified to pH 4. Finally, an organic substrate (propan-2-ol) was used as sacrificial electron donor and the deaerated aqueous solution was then placed under visible light irradiation (> 400 nm). The light

assisted formation of silver nanoparticles was followed by observing the growth of their plasmon band as a function of irradiation time.

As shown in Figure 4. A, the silver plasmon band quickly starts growing around 450 nm upon light exposure. After 200 min of irradiation, the optical absorption spectra do not evolve any more, indicating the end of the reaction and the total reduction of Ag^+ ions into Ag_n clusters. The plasmon band is broad and asymmetrically elongated towards the low energy side of the spectrum. The molar extinction coefficient per Ag^0 atom is evaluated to be around 4400 dm^3 mol^{-1} cm^{-1} at the peak maximum (460 nm). This spectral feature indicates the formation of large particles of non-spherical shape and/or with a heterogeneous size distribution. The plot of the time evolution of the absorbencies at the wavelength corresponding to the maximum of the plasmon band (Fig 4 .B, 460 nm) allows us to follow the formation of silver clusters and to estimate the initial photoreduction rate which is found to be around 2×10^{-6} mol L^{-1} min^{-1}. This value is of the same order of magnitude as those determined for Ag^+ ions photoreduction by $\{P_2W_{18}\}$ alone under UV illumination [22].

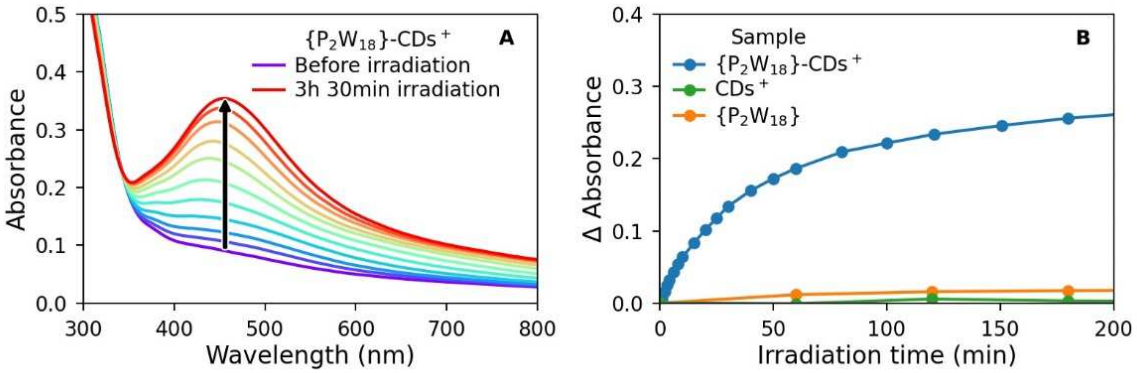

Fig. 4. A) UV-vis absorption spectra measured under visible illumination of a deaereted aqueous solution of 40 µM of Ag_2SO_4 containing 10 µM of $\{P_2W_{18}\}$, **25 mg L^{-1}** of CDs and 0.13 M of propan-2-ol. **B)** Temporal evolution of the absorbance at 460 nm during visible illumination of the previous solution.

The HR-TEM images (Fig 5. A) confirm the formation of silver nanoparticles upon illumination. The nanoparticles we obtained possess mono- or poly-crystalline structure and are quite inhomogeneous in shape and size (between 20 and 100 nm) in accordance with the shape of their plasmon band. We can then measure the observed plane spacing by calculating the FFT of the image of selected particles (Fig 5. B to E). Most nanoparticles, both mono- and poly-crystalline, present a lattice spacing of 2.4 Å, corresponding to {111} reflections of face-centered cubic (fcc) silver (JCPDS file 04-0783). Lattice spacings equal to 2.0 and 1.4 Å can also be measured and are consistent with the {002} and {022} silver metal planes, respectively.

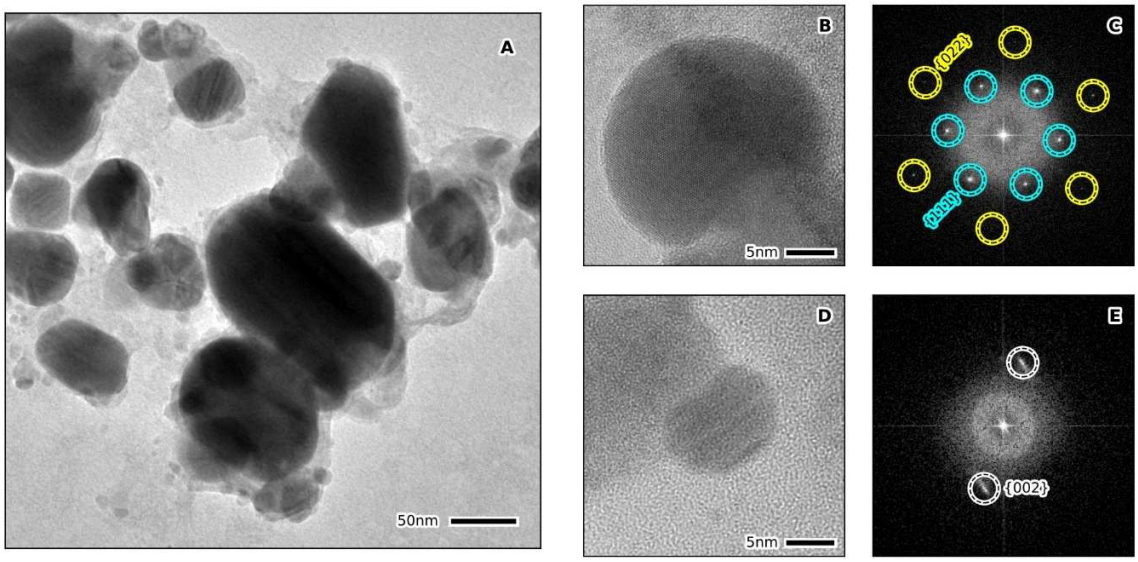

Fig. 5. A, B and D) HRTEM images of silver nanoparticles obtained during visible illumination of a deaerated solution of Ag_2SO_4 in the presence of CDs/$\{P_2W_{18}\}$ complex; **C and E)** FFT respectively calculated from (B) and (D); the planar distances responsible for the observed diffraction peaks are indicated.

Control experiments were carried out to check for photocatalytic activity of each single component of the system and when solutions were left in the dark without irradiation. When $\{P_2W_{18}\}$ was used without CDs, the absorption spectra did not show the growth of the plasmon band **(Fig. S1 and 4. B)**, meaning

that $\{P_2W_{18}\}$ alone is not photoactive under visible irradiation. Irradiation of solution containing CDs without $\{P_2W_{18}\}$ leads to a non significant modification of the absorption spectra **(Fig. S1 and 4. B)**, indicating the concomitant action of POM and CDs when the photoreduction process occurs. Finally, when the solution of the CDs/$\{P_2W_{18}\}$ complex with Ag^+ ions was investigated without irradiation, no nanoparticles were formed. These control experiments prove that silver nanoparticles need light to start forming and that only CDs can absorb the provided visible radiation. **It can be mentioned that up-conversion phenomenon has been described in several articles to explain photosensibilization of CDs in the visible** [40,41]**. Nevertheless, the CDs used in this work present directly a high absorbance at the blue end of the visible spectrum reaching up to 500 nm. Moreover, a complete study of the fluorescence of these CDs has been published elsewhere, and no up-conversion effect has been observed. So, to explain the photosensibilization in the visible domain we can assume a direct absorption in the absorption band in the visible part of the spectrum.**

According to our previous results, an efficient electron transfer can then occur between excited CDs and $\{P_2W_{18}\}$ [21]. This electron transfer provides precious insight on the Ag^+ reduction mechanism. Indeed, this electron transfer leads to the reduction of POM and consequently to the oxidation of CDs:

$$\boldsymbol{POM - CDs \overset{h\nu}{\rightarrow} POM^{x-} - CDs^{x+}}$$

Then CDs should be regenerated by scavenging an electron from the propan-2-ol, leading to the formation of the alcohol radical $(CH_3)_2C^{\bullet}OH$:

$$\boldsymbol{CDs^{x+} + x\,(CH_3)_2CHOH \rightarrow CDs + x\,(CH_3)_2C^{\bullet}OH + x\,H^+}$$

However, the redox potential of (Ag^+/Ag^0) couple appears to be too low (E = -1.75 V / NHE [42,43]) to allow the direct reduction of Ag^+ ions by reduced $\{P_2W_{18}\}$. Indeed, whatever the reduction degree of the POM, the thermodynamic is not favorable since the redox potentials of the POM couples vary from 0.1 V down at most to -0.9 V / NHE. Nevertheless, Ag^+ ions can complex with the alcohol radical according the reaction [42]:

$$\boldsymbol{(CH_3)_2C^{\bullet}OH + Ag^+ \rightarrow [Ag(CH_3)_2C^{\bullet}OH]^+}$$

Then the formation of this complex may change the value of the redox potential of silver and make it favorable the Ag^+ reduction [42]:

$$[Ag(CH_3)_2C^{\bullet}OH]^+ + Ag^+ \rightarrow Ag_2{}^+ + (CH_3)_2CO + H^+$$

After this initial step, the association and coalescence of the Ag^+ ions with initial small Ag_n^+ clusters would drive the growth of the silver particles:

$$2\,Ag_2{}^+ \rightarrow Ag_4{}^{2+}$$

$$Ag_m{}^{y+} + Ag_p{}^{z+} \rightarrow Ag_{(m+p)}{}^{(y+z)+}$$

Indeed, as the redox potential of silver clusters increases with their nuclearity [43], the direct reduction of the Ag_n^+ clusters by the reduced POM becomes thermodynamically favorable:

$$POM^{x-} + Ag_n{}^{x+} \rightarrow Ag_n + POM$$

The mechanism illustrating the different steps involved in the reduction of silver ions from CDs/{P_2W_{18}} under visible illumination is summarized Scheme 1.

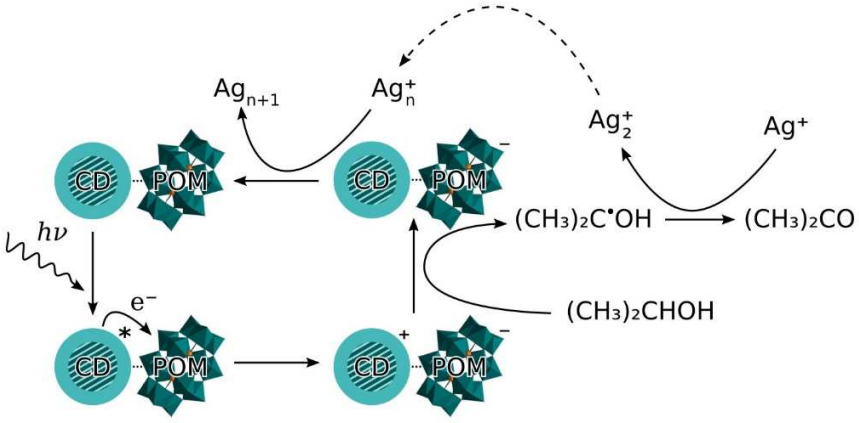

Scheme 1. Proposed mechanism explaining the reduction of silver ions from CDs/{P_2W_{18}} under visible illumination.

3.4. Photoreduction of Ag^+ ions using CDs/{$Co_4P_4W_{30}$} and CDs/{$Zn_4P_4W_{30}$} complexes

We have similarly investigated the photocatalytic activities of the two other CDs/POM complexes obtained from tetranuclear Dawson-derived sandwich POMs. Photocatalytic tests have been performed under the same experimental conditions. Figures 6. A and B show the absorption spectra recorded during the visible illumination of the two solutions containing CDs, POMs, Ag^+ ions and propan-2-ol at the previously indicated concentrations. In both cases, the reduction of Ag^+ ions is evidenced by the appearance of the plasmon band of silver nanoparticles around 420 nm and its intensity increase over the time reaction. The blue-shift of the plasmon band compared to the one obtained using {P_2W_{18}} indicates the formation of smaller nanoparticles. Moreover, this plasmon band exhibits a more sharped shape compared to that observed during the previous experiment with {P_2W_{18}}, with a higher molar extinction coefficient value (10000 and 7500 $dm^3\ mol^{-1}\ cm^{-1}$, respectively for {$Co_4P_4W_{30}$} and {$Zn_4P_4W_{30}$}). This feature usually traduces a reduction of the size of the nanoparticles. The TEM images finally confirm the formation of smaller silver nanoparticles, with sizes ranging between 10 and 50 nm (Fig. 6. C and D).

By observing the time evolution of the absorbance at the maximum of the plasmon band at 420 nm (Fig. 7), we can estimate the initial rate of Ag^+ ions reduction to be $5{,}3 \times 10^{-6}$ mol L^{-1} min^{-1}, which is higher to the kinetic rate measured with the POM {P_2W_{18}}. As a consequence, it appears that the Dawson-derived sandwich POMs {$Co_4P_4W_{30}$} and {$Zn_4P_4W_{30}$} promote much more effectively the nucleation phase of the silver nanoparticles compared to the Dawson POM {P_2W_{18}}, probably because of their ability to exchange a larger number of electrons.

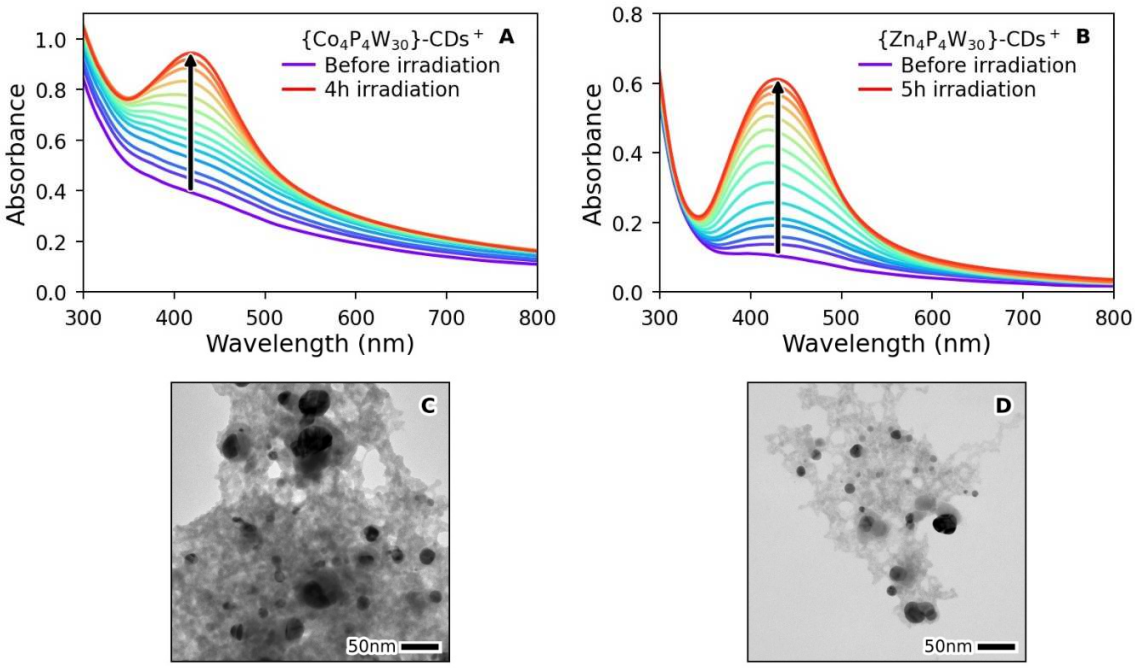

Fig. 6. UV-vis absorption spectra measured under visible illumination of a deaerated aqueous solution of 40 µM of Ag_2SO_4 containing 10 µM of **A)** $\{Co_4P_4W_{30}\}$ or **B)** $\{Zn_4P_4W_{30}\}$, **25 mg L^{-1}** of CDs and 0.13 M of propan-2-ol; HRTEM images of silver nanoparticles obtained during visible illumination of a deaerated solution of Ag_2SO_4 in the presence of **C)** CDs/$\{Co_4P_4W_{30}\}$ and **D)** CDs/$\{Zn_4P_4W_{30}\}$ complexes.

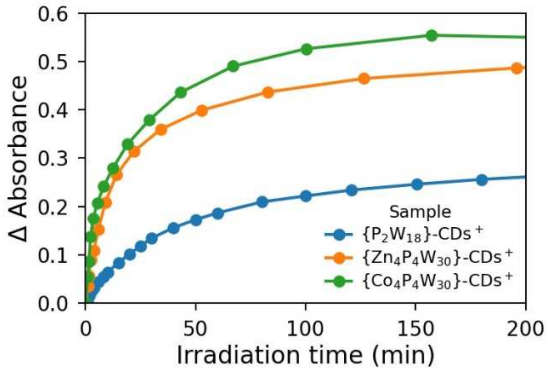

Fig. 7. Temporal evolution of the absorbance at 420 nm during visible illumination of the previous silver solutions using CDs/$\{Co_4P_4W_{30}\}$ and CDs/$\{Zn_4P_4W_{30}\}$ complexes as catalysts.

As before, control experiments using {$Co_4P_4W_{30}$} (Fig. S2) **and {$Zn_4P_4W_{30}$}** (Fig. S3) **alone have also been performed, but the absorption spectra did not show the growth of the plasmon band, meaning that these two POMs are not photoactive under visible irradiation when used alone.**

4. Conclusion

To conclude, we have managed to show how CDs/POM complexes are versatile hybrid devices capable of an applicative electron transfer. Through the photoreduction of silver ions we have been able to demonstrate how CDs can act as electron relays to enhance the catalytic performances of several POMs. This kind of evidence shows we have been successful in photosensitizing POMs *via* CDs.

This leaves us very optimistic on the wide array of the applicative possibilities of our hybrids. For example, due to the wide range of POM structures having well defined photocatalytic properties [44–46], such new POM-CDs complexes could be used in water depollution processes for the reduction and recovery of valuable heavy metals as well as in the reduction of protons into hydrogen. Moreover, reactions involving the reduction of metals could also be combined with the degradation of organic pollutants in place of a sacrificial electron donor. More generally, we open the route to consider CDs as a new family of cheap and environmentally friendly photosensitizers for photocatalytic applications.

Acknowledgments

This work was supported by Université de Paris and CNRS (Centre National de Recherche Scientifique). This project has received funding from the ANR (Agence Nationale de la Recherche) (Project POMDOT, postdoctoral fellowship to M.M.-S.), the city of Paris and the European Union's Horizon 2020 research and innovation program under Marie Sklodowska-Curie Grant Agreement 665850 (Ph.D. fellowship to A.M.).

[1] N. Serpone, A.V. Emeline, Semiconductor Photocatalysis — Past, Present, and Future Outlook, J. Phys. Chem. Lett. 3 (2012) 673–677. https://doi.org/10.1021/jz300071j.

[2] C. Xu, P. Ravi Anusuyadevi, C. Aymonier, R. Luque, S. Marre, Nanostructured materials for photocatalysis, Chem. Soc. Rev. 48 (2019) 3868–3902. https://doi.org/10.1039/C9CS00102F.

[3] H. Yang, A short review on heterojunction photocatalysts: Carrier transfer behavior and photocatalytic mechanisms, Mater. Res. Bull. 142 (2021) 111406. https://doi.org/10.1016/j.materresbull.2021.111406.

[4] C. Byrne, G. Subramanian, S.C. Pillai, Recent advances in photocatalysis for environmental applications, J. Environ. Chem. Eng. 6 (2018) 3531–3555. https://doi.org/10.1016/j.jece.2017.07.080.

[5] Y. Gao, K. Qian, B. Xu, Z. Li, J. Zheng, S. Zhao, F. Ding, Y. Sun, Z. Xu, Recent advances in visible-light-driven conversion of CO2 by photocatalysts into fuels or value-added chemicals, Carbon Resour. Convers. 3 (2020) 46–59. https://doi.org/10.1016/j.crcon.2020.02.003.

[6] M. Matsuoka, M. Kitano, M. Takeuchi, K. Tsujimaru, M. Anpo, J.M. Thomas, Photocatalysis for new energy production, Catal. Today. 122 (2007) 51–61. https://doi.org/10.1016/j.cattod.2007.01.042.

[7] J. Zhang, W. Hu, S. Cao, L. Piao, Recent progress for hydrogen production by photocatalytic natural or simulated seawater splitting, Nano Res. 13 (2020) 2313–2322. https://doi.org/10.1007/s12274-020-2880-z.

[8] J.-H. Shon, T.S. Teets, Molecular Photosensitizers in Energy Research and Catalysis: Design Principles and Recent Developments, ACS Energy Lett. 4 (2019) 558–566. https://doi.org/10.1021/acsenergylett.8b02388.

[9] T. Kawawaki, Y. Negishi, H. Kawasaki, Photo/electrocatalysis and photosensitization using metal nanoclusters for green energy and medical applications, Nanoscale Adv. 2 (2020) 17–36. https://doi.org/10.1039/C9NA00583H.

[10] X. Xu, R. Ray, Y. Gu, H.J. Ploehn, L. Gearheart, K. Raker, W.A. Scrivens, Electrophoretic Analysis and Purification of Fluorescent Single-Walled Carbon Nanotube Fragments, J. Am. Chem. Soc. 126 (2004) 12736–12737. https://doi.org/10.1021/ja040082h.

[11] Y.-P. Sun, B. Zhou, Y. Lin, W. Wang, K.A.S. Fernando, P. Pathak, M.J. Meziani, B.A. Harruff, X. Wang, H. Wang, P.G. Luo, H. Yang, M.E. Kose, B. Chen, L.M. Veca, S.-Y. Xie, Quantum-Sized Carbon Dots for Bright and Colorful Photoluminescence, J. Am. Chem. Soc. 128 (2006) 7756–7757. https://doi.org/10.1021/ja062677d.

[12] H. Aliyeva, A. Gurel, S. Nowak, S. Lau, P. Decorse, S. Chaguetmi, D. Schaming, S. Ammar, Photo-anodes based on TiO2 and carbon dots for photo-electrocatalytical measurements, Mater. Lett. 250 (2019) 119–122. https://doi.org/10.1016/j.matlet.2019.02.131.

[13] W. Shi, F. Guo, C. Zhu, H. Wang, H. Li, H. Huang, Y. Liu, Z. Kang, Carbon dots anchored on octahedral CoO as a stable visible-light-responsive composite photocatalyst for overall water splitting, J. Mater. Chem. A. 5 (2017) 19800–19807. https://doi.org/10.1039/C7TA06077G.

[14] X. Yu, J. Liu, Y. Yu, S. Zuo, B. Li, Preparation and visible light photocatalytic activity of carbon quantum dots/TiO2 nanosheet composites, Carbon. 68 (2014) 718–724. https://doi.org/10.1016/j.carbon.2013.11.053.

[15] S. Xie, H. Su, W. Wei, M. Li, Y. Tong, Z. Mao, Remarkable photoelectrochemical performance of carbon dots sensitized TiO 2 under visible light irradiation, J Mater Chem A. 2 (2014) 16365–16368. https://doi.org/10.1039/C4TA03203A.

[16] H. Li, R. Liu, Y. Liu, H. Huang, H. Yu, H. Ming, S. Lian, S.-T. Lee, Z. Kang, Carbon quantum dots/Cu2O composites with protruding nanostructures and their highly efficient (near) infrared photocatalytic behavior, J. Mater. Chem. 22 (2012) 17470. https://doi.org/10.1039/c2jm32827e.

[17] H. Zhang, H. Ming, S. Lian, H. Huang, H. Li, L. Zhang, Y. Liu, Z. Kang, S.-T. Lee, Fe2O3/carbon quantum dots complex photocatalysts and their enhanced photocatalytic activity under visible light, Dalton Trans. 40 (2011) 10822. https://doi.org/10.1039/c1dt11147g.

[18] J. Zhang, Y. Guo, Y. Xiong, D. Zhou, S. Dong, An environmentally friendly Z-scheme WO3/CDots/CdS heterostructure with remarkable photocatalytic activity and anti-photocorrosion performance, J. Catal. 356 (2017) 1–13. https://doi.org/10.1016/j.jcat.2017.09.021.

[19] G. Wei, X. Zhao, K. Du, Z. Wang, M. Liu, S. Zhang, S. Wang, J. Zhang, C. An, A general approach to 3D porous CQDs/MxOy (M = Co, Ni) for remarkable performance hybrid supercapacitors, Chem. Eng. J. 326 (2017) 58–67. https://doi.org/10.1016/j.cej.2017.05.127.

[20] G. Wei, K. Du, X. Zhao, Z. Wang, M. Liu, C. Li, H. Wang, C. An, W. Xing, Carbon quantum dot-induced self-assembly of ultrathin Ni(OH)2 nanosheets: A facile method for fabricating three-dimensional porous hierarchical composite micro-nanostructures with excellent supercapacitor performance, Nano Res. 10 (2017) 3005–3017. https://doi.org/10.1007/s12274-017-1516-4.

[21] A. Madonia, M. Martin-Sabi, A. Sciortino, S. Agnello, M. Cannas, S. Ammar, F. Messina, D. Schaming, Highly Efficient Electron Transfer in a Carbon Dot–Polyoxometalate Nanohybrid, J. Phys. Chem. Lett. 11 (2020) 4379–4384. https://doi.org/10.1021/acs.jpclett.0c01078.

[22] C. Costa-Coquelard, D. Schaming, I. Lampre, L. Ruhlmann, Photocatalytic reduction of Ag2SO4 by the Dawson anion α-[P2W18O62]6− and tetracobalt sandwich complexes, Appl. Catal. B Environ. 84 (2008) 835–842. https://doi.org/10.1016/j.apcatb.2008.06.018.

[23] M. Bonchio, M. Carraro, M. Gardan, G. Scorrano, E. Drioli, E. Fontananova, Hybrid photocatalytic membranes embedding decatungstate for heterogeneous photooxygenation, Top. Catal. 40 (2006) 133–140. https://doi.org/10.1007/s11244-006-0115-5.

[24] A. Troupis, E. Gkika, T. Triantis, A. Hiskia, E. Papaconstantinou, Photocatalytic reductive destruction of azo dyes by polyoxometallates: Naphthol blue black, J. Photochem. Photobiol. Chem. 188 (2007) 272–278. https://doi.org/10.1016/j.jphotochem.2006.12.022.

[25] A. Troupis, T.M. Triantis, E. Gkika, A. Hiskia, E. Papaconstantinou, Photocatalytic reductive–oxidative degradation of Acid Orange 7 by polyoxometalates, Appl. Catal. B Environ. 86 (2009) 98–107. https://doi.org/10.1016/j.apcatb.2008.08.001.

[26] A.M. Khenkin, I. Efremenko, L. Weiner, J.M.L. Martin, R. Neumann, Photochemical Reduction of Carbon Dioxide Catalyzed by a Ruthenium-Substituted Polyoxometalate, Chem. - Eur. J. 16 (2010) 1356–1364. https://doi.org/10.1002/chem.200901673.

[27] S. Antonaraki, T.M. Triantis, E. Papaconstantinou, A. Hiskia, Photocatalytic degradation of lindane by polyoxometalates: Intermediates and mechanistic aspects, Catal. Today. 151 (2010) 119–124. https://doi.org/10.1016/j.cattod.2010.02.017.

[28] T.S. Symeonidis, A. Athanasoulis, R. Ishii, Y. Uozumi, Y.M.A. Yamada, I.N. Lykakis, Photocatalytic Aerobic Oxidation of Alkenes into Epoxides or Chlorohydrins Promoted by a Polymer-Supported Decatungstate Catalyst, ChemPhotoChem. 1 (2017) 479–484. https://doi.org/10.1002/cptc.201700079.

[29] S. Li, G. Li, P. Ji, J. Zhang, S. Liu, J. Zhang, X. Chen, A Giant Mo/Ta/W Ternary Mixed-Addenda Polyoxometalate with Efficient Photocatalytic Activity for Primary Amine Coupling, ACS Appl. Mater. Interfaces. 11 (2019) 43287–43293. https://doi.org/10.1021/acsami.9b16694.

[30] D. Schaming, C. Costa-Coquelard, S. Sorgues, L. Ruhlmann, I. Lampre, Photocatalytic reduction of Ag2SO4 by electrostatic complexes formed by tetracationic zinc porphyrins and tetracobalt Dawson-derived sandwich polyanion, Appl. Catal. Gen. 373 (2010) 160–167. https://doi.org/10.1016/j.apcata.2009.11.010.

[31] D. Schaming, R. Farha, H. Xu, M. Goldmann, L. Ruhlmann, Formation and Photocatalytic Properties of Nanocomposite Films Containing Both Tetracobalt Dawson-Derived Sandwich Polyanions and Tetracationic Porphyrins, Langmuir. 27 (2011) 132–143. https://doi.org/10.1021/la1024923.

[32] D. Schaming, C. Allain, R. Farha, M. Goldmann, S. Lobstein, A. Giraudeau, B. Hasenknopf, L. Ruhlmann, Synthesis and Photocatalytic Properties of Mixed Polyoxometalate−Porphyrin Copolymers Obtained from Anderson-Type Polyoxomolybdates, Langmuir. 26 (2010) 5101–5109. https://doi.org/10.1021/la903564d.

[33] J.J. Walsh, J. Zhu, A.M. Bond, R.J. Forster, T.E. Keyes, Visible light sensitized photocurrent generation from electrostatically assembled thin films of [Ru(bpy)3]2+ and the polyoxometalate γ*-[W18O54(SO4)2]4−: Optimizing performance in a low electrolyte medium, J. Electroanal. Chem. 706 (2013) 93–101. https://doi.org/10.1016/j.jelechem.2013.07.020.

[34] B. Matt, J. Fize, J. Moussa, H. Amouri, A. Pereira, V. Artero, G. Izzet, A. Proust, Charge photo-accumulation and photocatalytic hydrogen evolution under visible light at an iridium(iii)-photosensitized polyoxotungstate, Energy Environ. Sci. 6 (2013) 1504. https://doi.org/10.1039/c3ee40352a.

[35] S. Schönweiz, M. Heiland, M. Anjass, T. Jacob, S. Rau, C. Streb, Experimental and Theoretical Investigation of the Light-Driven Hydrogen Evolution by Polyoxometalate-Photosensitizer Dyads, Chem. - Eur. J. 23 (2017) 15370–15376. https://doi.org/10.1002/chem.201702116.

[36] L. Wang, Y. Wang, T. Xu, H. Liao, C. Yao, Y. Liu, Z. Li, Z. Chen, D. Pan, L. Sun, M. Wu, Gram-scale synthesis of single-crystalline graphene quantum dots with superior optical properties, Nat. Commun. 5 (2014) 5357. https://doi.org/10.1038/ncomms6357.

[37] R. Contant, W.G. Klemperer, O. Yaghi, Potassium Octadecatungstodiphosphates(V) and Related Lacunary Compounds, in: A.P. Ginsberg (Ed.), Inorg. Synth., John Wiley & Sons, Inc., Hoboken, NJ, USA, 2007: pp. 104–111. https://doi.org/10.1002/9780470132586.ch18.

[38] R.G. Finke, M.W. Droege, P.J. Domaille, Trivacant heteropolytungstate derivatives. 3. Rational syntheses, characterization, two-dimensional tungsten-183 NMR, and properties of tungstometallophosphates P2W18M4(H2O)2O6810- and P4W30M4(H2O)2O11216- (M = cobalt, copper, zinc), Inorg. Chem. 26 (1987) 3886–3896. https://doi.org/10.1021/ic00270a014.

[39] M. Perikala, A. Bhardwaj, Excellent color rendering index single system white light emitting carbon dots for next generation lighting devices, Sci. Rep. 11 (2021) 11594. https://doi.org/10.1038/s41598-021-91074-w.

[40] Y. Zhang, M. Park, H.Y. Kim, B. Ding, S.-J. Park, A facile ultrasonic-assisted fabrication of nitrogen-doped carbon dots/BiOBr up-conversion nanocomposites for visible light photocatalytic enhancements, Sci. Rep. 7 (2017) 45086. https://doi.org/10.1038/srep45086.

[41] S. Huang, Q. Zhang, P. Liu, S. Ma, B. Xie, K. Yang, Y. Zhao, Novel up-conversion carbon quantum dots/α-FeOOH nanohybrids eliminate tetracycline and its related drug resistance in visible-light responsive Fenton system, Appl. Catal. B Environ. 263 (2020) 118336. https://doi.org/10.1016/j.apcatb.2019.118336.

[42] A. Henglein, The Reactivity of Silver Atoms in Aqueous Solutions (A γ-Radiolysis Study), Berichte Bunsenges. Für Phys. Chem. 81 (1977) 556–561. https://doi.org/10.1002/bbpc.19770810604.

[43] J. Belloni, Nucleation, growth and properties of nanoclusters studied by radiation chemistry, Catal. Today. 113 (2006) 141–156. https://doi.org/10.1016/j.cattod.2005.11.082.

[44] E. Gkika, A. Troupis, A. Hiskia, E. Papaconstantinou, Photocatalytic Reduction and Recovery of Mercury by Polyoxometalates, Environ. Sci. Technol. 39 (2005) 4242–4248. https://doi.org/10.1021/es0493143.

[45] H. Lv, W. Guo, K. Wu, Z. Chen, J. Bacsa, D.G. Musaev, Y.V. Geletii, S.M. Lauinger, T. Lian, C.L. Hill, A Noble-Metal-Free, Tetra-nickel Polyoxotungstate Catalyst for Efficient Photocatalytic Hydrogen Evolution, J. Am. Chem. Soc. 136 (2014) 14015–14018. https://doi.org/10.1021/ja5084078.

[46] R. Dehghani, S. Aber, F. Mahdizadeh, Polyoxometalates and Their Composites as Photocatalysts for Organic Pollutants Degradation in Aqueous Media-A Review, CLEAN - Soil Air Water. 46 (2018) 1800413. https://doi.org/10.1002/clen.201800413.